Vol. 19, No. 3 (2020) 1363-1373
Revista Mexicana de Ingeniería Química

A new route for the synthesis of $Sn_3Sb_2S_6$ thin films by chemical deposition

Una ruta nueva para la síntesis de películas delgadas de $Sn_3Sb_2S_6$ por depósito químico

E. Barrios-Salgado1[1]*, Y. Rodríguez-Lazcano[1], J. P. Pérez-Orozco[2] and A. R. Garcia-Angelmo[3]

[1]*Unidad Académica de Ciencias Básicas e Ingeniería, Universidad Autónoma de Nayarit, Ciudad de la Cultura "Amado Nervo" S/N, C. P. 63155, Tepic, Nayarit, México.*

[2]*Departamento de Ingeniería Química y Bioquímica, Instituto Tecnológico de Zacatepec, Tecnológico Nacional de México. Calzada Tecnológico # 27, Col. Centro. C. P. 62780, Zacatepec, Morelos. México.*

[3]*Centro Regional de Educación Superior Campus Cruz Grande, Universidad Autónoma de Guerrero, Carretera Ayutla-Cruz Grande SN, Col 6 de marzo, Comunidad Cruz Grande, Municipio Florencio Villarreal, C. P. 41800, Guerrero, México.*

Received: December 4, 2019; Accepted: February 6, 2020.

Abstract

In this work, SnS-Sn_2S_3 stack films were formed by sequential chemical deposition, and then they were annealed in a nitrogen atmosphere to synthesize $Sn_3Sb_2S_6$ thin films successfully. The structural and optical properties were studied by X-ray diffraction and transmittance and reflectance. All the samples show a high absorption coefficient of $> 10^5$ cm^{-1} in the visible region. Their optical bandgap and refractive index are between 1.6-1.8 eV and 3.00-2.71, respectively, which decrease with the increase of film thickness. The electrical conductivity is in the range of 10^{-8} to 10^{-7} Ω^{-1} cm^{-1}. The light-generated current density (J_L) is presented as a function of $Sn_3Sb_2S_6$ film thickness when exposed to air mass 1.5 global (AM1.5G) and solar radiation intensity of 1000 W/m^2. In short, $Sn_3Sb_2S_6$ thin films obtained via the proposed new route exhibit appropriate properties for solar cell applications.

Keywords: Sulfosalt thin films, chemical deposition, $Sn_3Sb_2S_6$, thermal annealing process.

Resumen

En este trabajo, las bicapas de SnS-Sn_2S_3 fueron formadas usando depósitos químicos secuenciales, posteriormente éstas fueron horneadas en atmosfera de nitrógeno para sintetizar satisfactoriamente las películas delgadas de $Sn_3Sb_2S_6$. Las propiedades estructurales y ópticas fueron analizadas por difracción de rayos X y transmitancia y reflectancia. Todas las películas obtenidas muestran un alto coeficiente de absorción $>10^5$ cm^{-1} en la región visible. La brecha óptica de energía y el índice de refracción están entre 1.6-1.8 eV y 3.00-2.71, respectivamente, los cuales disminuyen con el aumento del espesor de la película. La conductividad eléctrica está en el intervalo de 10^{-8} a 10^{-7} Ω^{-1} cm^{-1}. La densidad de corriente generada por la luz (J_L) se presenta como una función del espesor de la película $Sn_3Sb_2S_6$ cuando se expone a una radiación solar global con masa de aire de 1.5 (AM1.5G) de intensidad 1000 W/m^2. En pocas palabras, las películas delgadas de $Sn_3Sb_2S_6$ obtenidas vía la ruta novedosa propuesta, exhiben propiedades adecuadas para aplicaciones en celdas solares.

Palabras clave: Películas delgadas de sulfosales, depósito químico, $Sn_3Sb_2S_6$, tratamiento térmico.

1 Introduction

In the last years, the sulfosalt layers have attracted attention due to their good optoelectronic properties, which give them a great potential to be used in solar cell, sensors, and thermoelectric energy conversions (Boldish and White, 1998; Dittrich *et al*. 2009; Gassoumi, A., Kanzari, 2011; Musgraves *et al*., 2011; Ben Rabeh *et al*., 2015). The sulfosalts can be defined as IV-V-VI ternary compounds. Additionally, quaternary and more complex compounds can be obtained by introducing transition metals through coupled isoelectronic substitution (Dittrich *et al*., 2007). Among the materials investigated, tin antimony sulfide (TAS) thin films have a significant interest due not only because they have a band gap energy from 1.2 to 2.5 eV with absorption coefficient above 10^5 cm^{-1}, appropriate for photovoltaic and photonic applications, but also for its abundance in nature, non-toxic and low-cost constituents, and reasonably good performance (Khan *et al*., 2016; Aousgi and Kanzari, 2011; Khemiri *et al*., 2018; Abdelkader *et al*., 2014; Drissi *et al*. 2013; Ali *et al*., 2017; Tlig *et al*. 2017).

* *Corresponding author. E-mail*: enue.barrios@uan.edu.mx
https://doi.org/10.24275/rmiq/Mat1061
issn-e: 2395-8472

The TAS materials have prepared by different methods such vacuum evaporation process, thermal evaporation, electro-pyroelectric technique, pulsed laser deposition, electron beam, among others (Abdelkader *et al*., 2016, Abdelkader *et al*., 2018; Mellouki *et al*., 2018; Jebali *et al*., Chalapathi *et al*., 2018; 2016; Dittrich *et al*., 2009; Bennaji, *et al*. 2019, Gassoumi *et al*., 2015). However, chemical bath deposition is simple method widely used to obtain semiconductor thin films on substrates due to some advantages, such as large deposition area, reproducibility, low cost equipment and law temperature processes (Lee *et al*., 2008 and 2009; Hodes, 2003 and 2007). In addition, combinatorial techniques have also been contributed to enhance part to obtain an appropriate semiconductor (Ali *et al*., 2016; Ovando-Medina *et al*., 2018).

Recent studies have been focused in the ternary compound $Sn_3Sb_2S_6$ because its thin films have shown a good transmission, strong absorption coefficients, a band gap energy close to the theoretical optimum for efficient conversion of solar radiation into electrical power, and a resistive hysteresis behavior (Larbi *et al*., 2014a; Fadhli *et al*., 2016). These properties confer to this material great importance in photovoltaic, optical storage, and solar applications. Thin films of $Sn_3Sb_2S_6$ were deposited by vacuum thermal evaporation (Larbi *et al*., 2014a and 2014b). The authors found that the optical band gap varies from 1.18 to 1.75 eV, and the absorption coefficients were in the range of 10^4 and 10^6 cm^{-1}, as a function of thicknesses and temperature substrates. Also, the films shows preferential growth in the (416) plane. The same authors synthesized $Sn_3Sb_2S_6$ thin films by an oblique angle deposition method, obtaining a direct band gap in the range of 1.44 eV to 1.66 eV and absorption coefficients from 10^5 to 10^6 cm^{-1} (Larbi *et al*., 2016). (SnS)m(Sb_2S_3)n thin films, including $Sn_3Sb_2S_6$, were prepared by thermal evaporation using the glancing angle deposition technique (Abdelkader *et al*., 2018), the $Sn_3Sb_2S_6$ thin films showed direct band gap of 1.67 eV, absorption coefficients of 10^5 cm^{-1} and photocurrent of 25 mA/cm^2 for the sample with a thickness of approximately 250 nm. Bennaji *et al*. (2019) obtained $Sn_3Sb_2S_6$ thin films via vacuum evaporation process followed by annealing process. They noticed that thermal conductivity and heat capacity values of the thin films increased by increasing annealing temperature, and the conductance was thermally activated, with an activation energy of about 0.813 eV. However, although thermal, electrical, and optical properties of $Sn_3Sb_2S_6$ thin films prepared by vacuum thermal evaporation and oblique angle deposition method were characterized over six years ago, little attention has been paid to obtain these thin films via CBD technique. For this reason, this work shows a new route for the synthesis of $Sn_3Sb_2S_6$ thin films using successive chemical deposits of Sb_2S_3 onto SnS thin films with a subsequent thermal annealing process. The chemical composition and the structural, electrical, and optical properties of these thin films are presented.

2 Materials and methods

2.1 *Thin films deposition*

Glass/SnS-Sb_2S_3 thin film stacks were prepared with two successive chemical bath deposition. First, SnS thin films were grown in corning glass following the methodology proposed by Nair *et al*. (2016). The deposition was carried out during 1 h 30 min, 3 h, and 4 h 30 min at 25 °C, which generates film thicknesses of 30, 50, and 70 nm, respectively. Afterward, the Sb_2S_3 thin film was stacked by deposition for 1 h 30 min, forming a thickness of this film of 250 nm, according to the procedure described by Rodríguez-Lazcano *et al*. (2005). Finally, the thin film stacks were treated by thermal annealing process for 30 min in N_2 atmosphere at 300 °C and 10 Torr to synthesize the $Sn_3Sb_2S_6$ thin films.

2.2 *Characterization*

The chemical composition of $Sn_3Sb_2S_6$ thin films was characterized in an Oxford X-act energy dispersive X-ray spectrum (EDX) analyzer attached to a Hitachi-SEM SU1510. X-ray diffraction (XRD) patterns were recorded on a Rigaku Ultima IV diffractometer with Cu-Kα (1.5406 Å) radiation at an incidence of 0.5, 1.5, and 2.0° with the sample plane. Such grazing incidence XRD (GIXRD) study helps to assess the structure and composition of the film along with its thickness.

The photocurrent response of the films was examined using a Keithley 230 programmable voltage source and Keithley 619 electrometer. The electrical measurements were performed using two silver-printed-electrodes of 5 mm long at 5 mm separation applied on the film surface and dried at 60 °C for 30 min. The current (I) in the films was recorded at each

0.5 s for the first 20 s in the dark to ensure the sample stabilization, the next 20 s under illumination and for the last 20 s after switching off the illumination, with a bias (V) of 100 V across the electrodes (established previously as ohmic region). A tungsten-halogen ELH lamp provides an intensity of 1000 W/m^2 on the plane of the film. Electrical conductivity (σ) of the $Sn_3Sb_2S_6$ thin films was estimated from the current and voltage values, the electrode geometry, and the film thickness.

Optical transmittance (T) and specular reflectance (R) spectra of the films were recorded for film-side incidence with air and a front aluminized mirror as references on a UV-VIS-NIR V-670 JASCO spectrophotometer. The optical absorption coefficient (α) was calculated with T and R values, considering multiple reflections within the thin films.

3 Results and discussion

3.1 Formation of ternary thin films

The conditions of successive deposition of Sb_2S_3 on SnS thin films previously grown onto a corning glass substrate, both by chemical bath deposition, allowed the formation of $Sn_3Sb_2S_6$ thin films. This fact was corroborated by EDX and XRD techniques, as shown in the following sections.

Starting from a 250 nm film of Sb_2S_3 and a SnS film of 30, 50 or 70 nm thickness; and from the mass densities and formula mass of SnS (5.13 g/cm^3 and 150.75 g/mol), Sb_2S_3 (4.72 g/cm^3 and 339.68 g/mol), and of $Sn_3Sb_2S_6$ (4.93 g/cm^3 and 792.02 g/mol) the thickness of the ternary compound film was estimate as 270, 291 and 312 nm, respectively. The basic stoichiometric reaction for the formation of $Sn_3Sb_2S_6$ from Sb_2S_3 and SnS thin films that takes place during the thermal annealing process is:

$$3\,SnS + Sb_2S_3 \xrightarrow{\Delta} Sn_3Sn_2S_6 \qquad (1)$$

3.2 Chemical composition

Figure 1 shows the EDX spectra for SnS (30, 50 or 70 nm) - Sb_2S_3 (250 nm) stack films annealed at 300°C for 30 min at 10 Torr in nitrogen atmosphere. EDX analysis show peaks due to Sb-L$_{\alpha 1}$ at 3.61 keV, Sn-L$_{\alpha 1}$ and Sn-L$_{beta2}$ at 3.44 and 3.90 keV, respectively and S-K$_{\alpha 1}$ at 2.31 keV. Also, the Na-K$_{\alpha 1-2}$ at 1.04 keV and Si- K$_{\alpha 1}$ at 1.74 keV identified peaks come from the substrate.

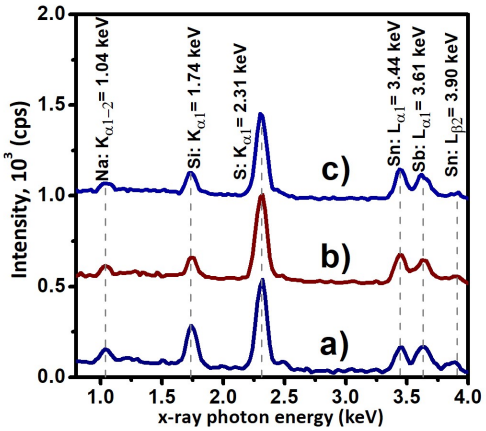

Fig. 1. EDX spectrum of $Sn_3Sb_2S_6$ for thickness of a) 270, b) 291, and c) 312 nm.

The intensity of Si is higher in figure 1a) because it corresponds to the sample with the smallest thickness. The relative intensity between the peaks of Sn, Sb and S was constant for all three samples, indicating that the atomic percentage is similar.

The elemental analysis by EDX software showed the following percentage of Sn, Sb and S: 2.64, 2.31, and 6.05% for sample with 270 nm of film thickness; 2.97, 1.98 and 6.05% for sample with 291 nm of film thickness; and 3.08, 1.87 and 6.05% for sample with 312 nm of film thickness. This suggests that SnS + Sb_2S_3 stack transforms to $Sn_3Sb_2S_6$ under annealing conditions. This result is corroborated by XRD analysis in the next section.

3.3 Structural properties

The Grazing Incidence X-Ray Diffraction (GIXRD) analysis was conducted by varying the angle of incidence to analyze the phases present throughout the thickness of the developed samples. The sampling depth (SD) is the depth into the film at which the intensity of x-rays entering the film at a grazing angle δ (angle between the beam and the film surface) drops to $1/e = 0.37$ of its initial value. The mass absorption coefficient (μ_{mass}), linear absorption coefficient (α), penetration depth (PD), and sampling depth (SD) concerning these angles were estimated following standard procedure (McCandless, 2005) using standard data (Hubbell and Seltzer, 2004). The procedure is described as follow:

- Elemental mass absorption coefficients (μ_{mass}) for Cu-Kα radiation (0.00824 MeV) are S, 89.1 cm^2/g; Sn, 256 cm^2/g; Sb, 270 cm^2/g.

- Atomic/formula mass (g/mol): S, 32.06; Sn, 118.71; Sb, 121.75; $Sn_3Sb_2S_6$, 792.02
- Formula mass fraction (X): $Sn_3Sb_2S_6$-S, 0.24; Sb, 0.31 and Sn, 0.45.
- Mass density (ρ): $Sn_3Sb_2S_6$, 4.93 g/cm^3.
- Mass absorption coefficient (μ_{mass}) of the substance for Cu-Kα radiation is: $\mu_{mass}(Sn_3Sb_2S_6)$, 219.76 (cm^2/g).

$$\mu_{mass} = [X(S)\cdot\mu_{mass}(S)] + [X(Sn)\cdot\mu_{mass}(Sn)] + [X(Sb)\cdot\mu_{mass}(Sb)] \quad (2)$$

- Linear absorption coefficient is

$$\alpha = rho{\cdot}\mu_{mass} = 4.93\frac{g}{cm^3}\cdot 219.76\frac{cm^2}{g} = 1083cm^{-1} \quad (3)$$

- Penetration depth (PD)

$$PD = \frac{1}{\alpha} = \frac{1}{1083cm^{-1}} = 9.23\mu m \quad (4)$$

- Sampling depth (SD)

$$SD = PD\cdot\sin(\delta) \quad (5)$$

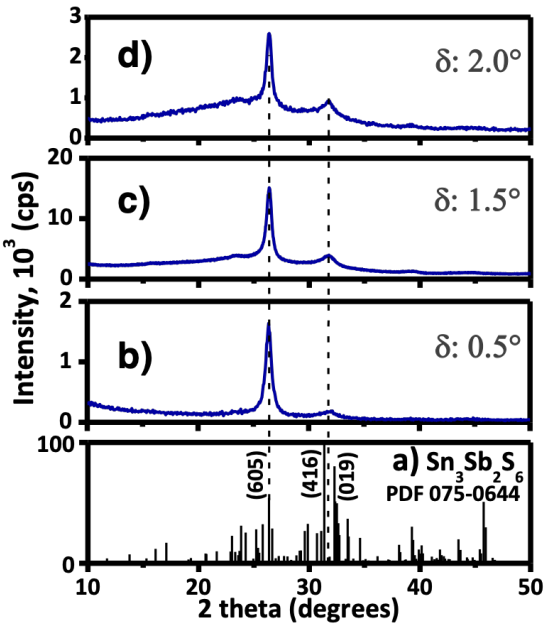

Fig. 2. XRD patters of: a) powder diffraction file data, and b), c), and d) $Sn_3Sb_2S_6$ film of 270 nm recorded at 0.5, 1.5, and 2.0 degrees, respectively.

Refractive index of the substance for the X-ray is approximated to 1 whereas it is 0.9999, mentioned for common semiconductors (McCandless, 2005). This requires $\delta > 0.3°$ for compound semiconductors to avoid total internal reflection of X-rays at the air-to-film interface.

The calculated sampling depths for $Sn_3Sb_2S_6$ thin film at different incidence angles were: SD (0.5º) = 80 nm, SD (1.5º) = 242 nm, and SD (2.0º) = 322 nm.

In figures 2, 3, and 4 the XRD patterns recorded at 0.5, 1.5, and 2.0 degrees for $Sn_3Sb_2S_6$ thin films of 270, 291, and 312 nm are shown. The diffractograms show XRD peaks matching well with the standard pattern of orthorhombic $Sn_3Sb_2S_6$ (PDF 075-0644) for all samples. According to the results, only a homogeneous $Sn_3Sb_2S_6$ phase was formed along the sample thickness. No secondary phases were observed. For incidence angles of 0.5 and 1.5 degrees the value of SD is 80 and 242 nm, respectively; therefore, it is not expected to see the contribution of the glass substrate, as shown in figures 2b) and c), 3b) and c), 4b) and c). On the other hand, in figures 2d), 3d) and 4d), the contribution of the glass substrate for an angle of incidence of 2.0 degrees is observed in the range 15-35º of 2θ. This fact is because the SD value is higher than the film thickness. In PDF 075-0644, the intensities of XRD peaks from the different planes are: (605), 54%; (416), 100%; (019), 80%. The broad peak centered at 2θ= 31.7º is observed in all cases, which is associated with the contribution of (416) and (019) planes. In all the patterns, the peak due to diffraction from (605) planes dominates. Thus, the preferred orientation along the (605) hkl plane was obtained for all three samples. The texture coefficient (TC) for the (605) crystalline planes was evaluated, as described in a previous article (McCandless, 2005). The values of TC are above 1, and decreases with the incidence angle. Previous works have reported a strong preferred orientation corresponding to (416) plane for samples synthesized by thermal evaporation (Larbi *et al*., 2014a, Larbi *et al*., 2014b & Larbi *et al*., 2016). Preferential growth seems to be determined by the growth technique, i.e., the growth conditions affect the structure of the material. The grain diameters values of the thin films were calculated based on the Debye-Scherrer's equation (Cullity and Stock, 2001). The grain diameters were in the range of 13-15 nm, which increases slightly with increasing the film thickness. The small crystal size obtained is common in films deposited by chemical deposition technique (Hodes, 2003). These results are shown in Table 1.

Table 1. Grain diameter and texture coefficient for $Sn_3Sb_2S_6$ thin films.

Sample	Texture coefficient (TC) (605)			Grain diameter (nm)
	0.5°	1.5°	2.0°	
270 nm	1.88	1.76	1.68	13
291 nm	1.73	1.65	1.60	15
312 nm	1.90	1.75	1.70	17

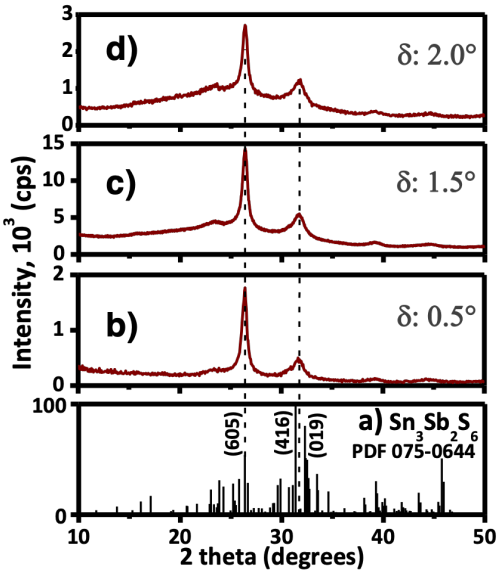

Fig. 3. XRD patters of: a) powder diffraction file data, and b), c), and d) $Sn_3Sb_2S_6$ film of 291 nm recorded at 0.5, 1.5, and 2.0 degrees, respectively.

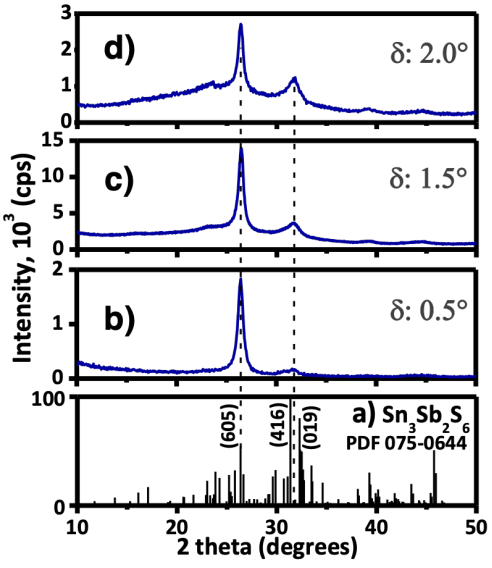

Fig. 4. XRD patters of: a) powder diffraction file data, and b), c), and d) $Sn_3Sb_2S_6$ film of 312 nm recorded at 0.5, 1.5, and 2.0 degrees, respectively.

3.4 Electrical properties

Figure 5 displays the photoconductivity response curves of the $Sn_3Sb_2S_6$ thin films. The thin films were slightly photoconductive. Electrical conductivity (σ) was estimated from the current and voltage values, the electrode geometry and the film thickness. The dark conductivity calculated were 0.11 10^{-7}, 0.55 10^{-7} and 1.77 10^{-7} $(\Omega\ cm)^{-1}$ for 270, 291 and 312 nm of film thickness, respectively. The increase in the electrical conductivity values with the thickness is related with the atomic percent of Sn in the chemical composition of $Sn_3Sb_2S_6$ thin film, as seen in the analysis of the chemical composition in section 3.2. According to our bibliographic search, there are no reports available on regarding the electrical conductivity of $Sn_3Sb_2S_6$ thin film. The electrical conductivity obtained in this work is hoped because it drops between the reported values for the binary starting materials, 10^{-9}-10^{-8} and 10^{-6} $(\Omega\ cm)^{-1}$ for Sb_2S_3 and SnS, respectively (Rodríguez-Lazcano *et al*., 2005 and Nair *et al*., 2016).

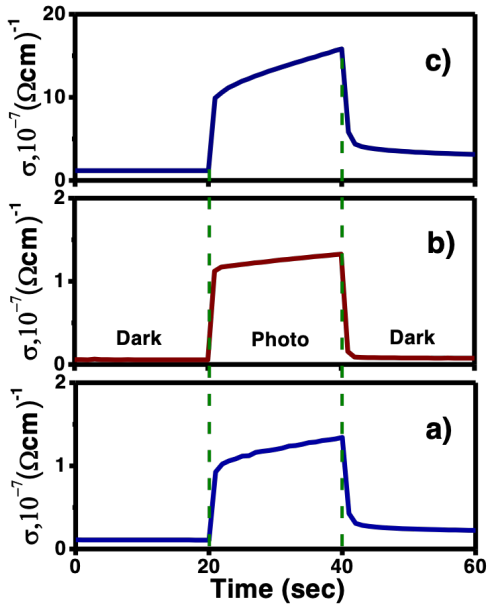

Fig. 5. Photoconductivity of $Sn_3Sb_2S_6$ thin films for thickness of a) 270, b) 291, and c) 312 nm.

3.5 Optical properties

The optical properties were recorded in the range between 500 and 2500 nm by measuring at normal incidence the transmittance (T) and reflectance (R). Figures 6 to 8 depict T, R and $T+R$ spectra and optical absorption coefficient (α) versus photon energy ($h\nu$) and $(\alpha h\nu)^{2/3}$ versus $h\nu$ of $Sn_3Sb_2S_6$ thin film developed. The value of $T+R$ at long wavelength was near 90-100% in the three samples, indicating no significant energy loss due to reflection. The average value of the reflectance toward the long wavelength for these films was 24.9, 23.6, and 21.0%, respectively (Fig. 6a), 7a), and 8a)).

To estimate the effective refractive index (n) of the films, the average optical reflectance in the long wavelength region, away from the region of band-to-band optical absorption was taken (Smith, 1978):

$$n = \left(1 + R^{1/2}\right)\left(1 - R^{1/2}\right) \tag{6}$$

An estimate for the film thickness was calculated by the wavelengths λ_1 and λ_2 corresponding to the adjacent crest and valley in the reflectance spectrum (Smith, 1978):

$$d = (\lambda_1 * \lambda_2)/2n(\lambda_1 - \lambda_2) \tag{7}$$

This estimation assumes near-uniform film composition and, therefore, nearly constant refractive index along the thickness of the films, which is expected due to the homogeneity of the $Sn_3Sb_2S_6$ phase. The refractive index decreased as increasing the film thickness from 3.0 to 2.71 (reported in Table 3). This fact may be attributed to the content of Sb and Sn present in the films, i. e. the atomic percent of Sb is higher in the thinnest film. The reported values for the high-frequency relative dielectric permittivity (ε_r) are 8.35 and 14.0 for Sb_2S_3 and SnS, respectively (Madelung, 1992). Hence, the n values calculated $\left(n = \varepsilon r^{1/2}\right)$ for the binary starting materials are 2.89 for Sb_2S_3 and 3.74 for SnS; this implies that the estimated values would be acceptable. The estimated thicknesses from equation (7) were 224, 245, and 265 nm. These values are comparable with 270, 291, and 312 nm obtained from the chemical equations in section 3.1 and cited as film thickness in this work. These values differ by less than 17%.

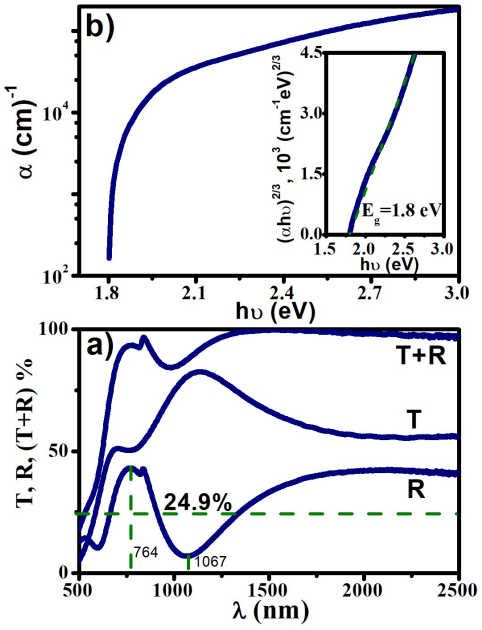

Fig. 6. a) T, R and $T + R$ spectra; and b) optical absorption coefficient (α) versus photon energy ($h\nu$) and $(\alpha h\nu)^{2/3}$ versus $h\nu$ (given as inset) of $Sn_3Sb_2S_6$ thin film of 270 nm in thickness.

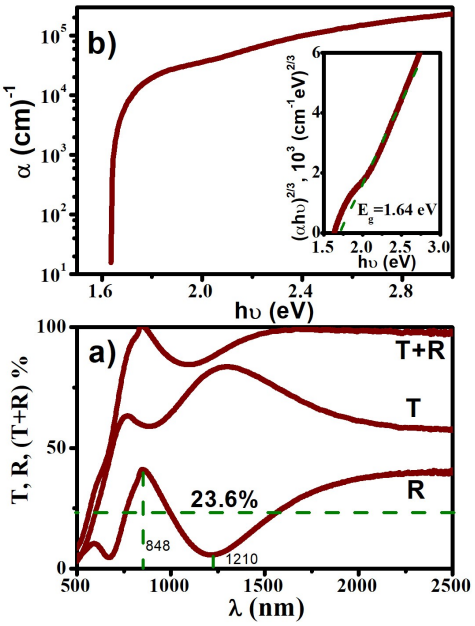

Fig. 7. a) T, R and $T + R$ spectra; and b) optical absorption coefficient (α) versus photon energy ($h\nu$) and ($\alpha h\nu$)2/3 versus $h\nu$ (given as inset) of $Sn_3Sb_2S_6$ thin film of 291 nm in thickness.

Table 2. Estimated thicknesses from reflectance spectra, refractive index (n) and bandgap energy (E_g) for $Sn_3Sb_2S_6$ thin films.

Sample	Estimated thickness (nm)	Refractive index (n)	E_g (eV)
270 nm	224	3.00	1.80
291 nm	245	2.89	1.64
312 nm	265	2.71	1.63

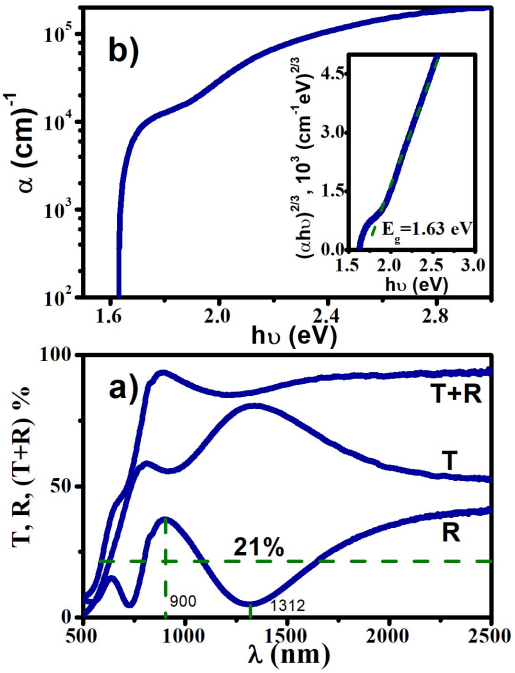

Fig. 8. a) T, R and $T + R$ spectra; and b) optical absorption coefficient (α) versus photon energy ($h\nu$) and $(\alpha h\nu)^{2/3}$ versus $h\nu$ (given as inset) of $Sn_3Sb_2S_6$ thin film of 312 nm in thickness.

The evaluation of α is reliable when the sum $T + R$ remains above 80% prior to the onset of strong optical absorption due to band-to band electronic transition. From the transmittance and reflectance spectra data (Fig. 6a, 7a and 8a) and film thickness (d), the optical absorption coefficient (α) as a function of the photon energy ($h\nu$) was estimated, by considering multiple reflections within the thin film, according to the following equation (Schroder, 1990):

$$\alpha = \frac{1}{d}\ln\left\{\frac{(1-R)^2}{2T} + \left[\left(\frac{(1-R)^2}{2T}\right)^2 + R^2\right]^{1/2}\right\} \quad (8)$$

Values of absorption coefficient higher than 10^5 cm^{-1} were obtained in the visible region, as can be seen in Fig. 6b), 7b) and 8b). This value is a good result for application in solar cells. The interpolation of these plots toward $\alpha \longrightarrow 0$ in the photon energy ($h\nu$) axis gives the optical band gap (E_g). To obtain the type of electronic transition which occurs during the optical absorption, ($\alpha h\nu$) is plotted versus $h\nu$ as shown in Fig. 6b), 7b) and 8b). The best fit is obtained for $(\alpha h\nu)^{2/3}$ versus $h\nu$ with a correlation factor of 0.99. From the linear regression analysis, the E_g values were calculated, which are in the range of 1.63 and 1.80 eV (see Table 2). These values are in agreement with the reported in the literature (Larbi *et al*., 2014b and Abdelkader *et al*., 2018). Plots of $(\alpha h\nu)^2$ or $(\alpha h\nu)^{1/2}$ versus $h\nu$ brings down the correlation factor to 0.96 or less, making the straight-line fit unacceptable, i. e., the linear fit establishes that the direct forbidden electronic transitions take place during the optical absorption (Smith, 1978).

The decrease in the values of E_g depends on the SnS thickness in the $Sn_3Sb_2S_6$ thin film formation, as seen in the analysis of the chemical composition (see section 3.2), which causes the formation of localized states in the gap of the samples. On the other hand, the slight increase in grain size as the function of the thickness, could be contributing to the reduction of the optical band gap.

3.6 *Light-generated current density*

The absorption coefficient, type and values of E_g have a direct consequence in the light-generated current density (J_L), which sets the upper limit for the short-circuit current density (J_{sc}) when a thin film of a particular semiconductor is used as an absorbent element in a solar cell, the current density generated was calculated by the following equation (Nelson, 2003 and Becerra, 2011):

$$J_L(mA/cm^2) = 0.1 * q * \int_{E_{g1}}^{\infty} N_{ph}(h)(1-e^{-\alpha_1 d_1})dE \quad (9)$$

The optical absorber film in the solar-cell structure sees the incident solar radiation (assumed for calculation as the air-mass 1.5 global spectra: AM1.5G of intensity 1000 W/m^2) as a source of photons with its flux density (N_{ph}) distributed over the wavelength as in Fig. 9a). Such data were obtained from the Standard Global AM1.5 spectrum Tables (Würfel, 2005), assuming that the thickness of the film is large.

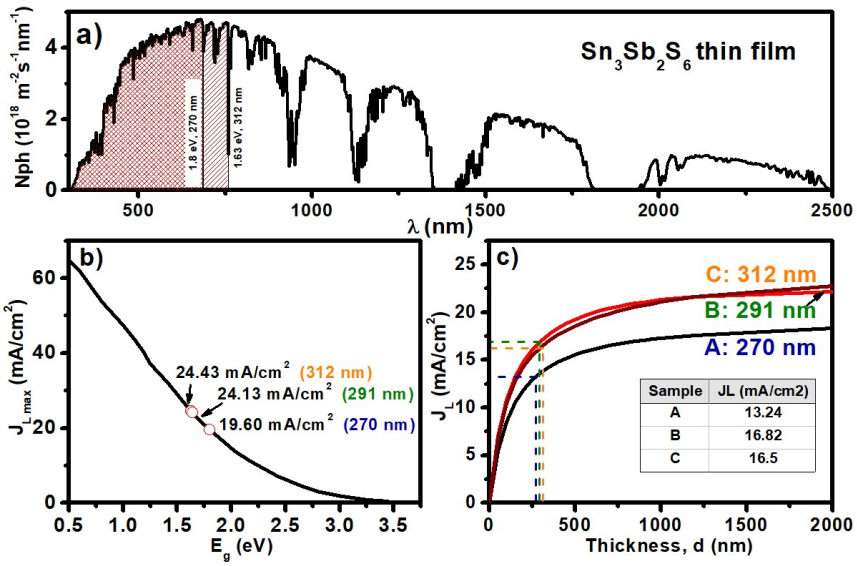

Fig. 9. a) Spectral distribution of photon flux density (N_{ph}) with wavelength (λ); b) maximum light-generated current density (J_{Lmax}) and c) light-generated current density (J_L) as a function of film thickness.

Hence, depending on the E_g, the photon flux density for the wavelength indicated in the shaded region for the semiconductor would produce a current density arising from an electron-hole generation for each absorbed photon of energy-E_g. It is also assumed that the electron-hole pairs are separated across the absorber without recombination; multiple exciton generation is ignored. These assumptions help place the J_{Lmax} values in Fig. 9b) for solar-cell absorbers of $Sn_3Sb_2S_6$ thin films of 270 nm (E_g=1.8 eV, Fig. 6b), 291 nm (E_g=1.64 eV, Fig. 7b), and 312 nm (E_g=1.63 eV, Fig. 8b) in thickness. Values of J_{Lmax} of for thickness to 270 nm, 291 nm, and 312 nm of $Sn_3Sb_2S_6$ are 19.60, 24.13, and 24.43 mA/cm^2, respectively, as indicated in Fig. 9b). Fig. 9c) shows the estimates values of J_L for $Sn_3Sb_2S_6$ thin films developed as a function of absorber film thickness, obtained using α versus $h\nu$ plots of Fig. 6b), 7b), and 8b). Variations of E_g and α with thickness, or of reflection losses at interfaces is not considered. The values for J_L are 13.24, 16.82, and 16.50 mA/cm^2 for 270, 291, and 312 nm in thickness, respectively. These results are good since the values are close to those of J_{max} estimated. The use of this material as an absorber in solar cells could generate good short circuit current (J_{SC}) values.

Conclusions

It can be concluded that $Sn_3Sb_2S_6$ thin films were successfully synthesized by chemical deposition route. The films were uniform and had good adherence to the substrate. Only a homogeneous $Sn_3Sb_2S_6$ phase is formed along with the thickness of the samples, which was corroborated by EDX and XRD analysis. The polycrystalline films show crystal size in the range of 13-15 nm with preferential orientation in the (605) plane, and they have a high absorption coefficient >10^5 cm^{-1} in the visible region. The optical bandgap of $Sn_3Sb_2S_6$ thin films is 1.80, 1.64, and 1.63 for 270, 291, and 312 nm in thickness. The refractive index decreases from 3.00 to 2.71 depending on the content of Sb and Sn present in the films. The electrical conductivity of these films is in the range of 10^{-8} - 10^{-7} Ω^{-1} cm^{-1}. Estimates values of J_L were 12.50, 15.02, and 16.98 mA/cm^2 for 270, 291, and 312 nm in thickness, respectively. Therefore, these results confirm that the chemical deposition route is a simple synthesis method for controlling the chemical composition and structure of $Sn_3Sb_2S_6$ with electrical and optical properties appropriate for solar cell applications.

Acknowledgements

We acknowledge to Patronato UAN through the project "Impulso a la Investigación". We thank IER-UNAM through CONACYT-LIFYCS 123122 for Infrastructure support.

References

Abdelkader, D., Akkari, F. C., Khemiri, N., Miloua, R., Antoni, F., Gallas, B., Kanzari, M. (2018). Effect of SnS addition on the morphological and optical properties of $(SnS)_m(Sb_2S_3)_n$ nanorods elaborated by glancing angle deposition. *Physica B: Condensed Matter 546*, 33-43. https://doi.org/10.1016/j.physb.2018.05.016

Abdelkader, D., Rabeh, M. B., Khemiri, N., Kanzari, M. (2014). Investigation on optical properties of $Sn_xSb_yS_z$ sulfosalts thin films. *Materials Science in Semiconductor Processing 21*, 14-19. https://doi.org/10.1016/j.mssp.2014.01.027

Ali, N., Hussain, A., Ahmed, R. Wan Shamsuri, W. N., Abdel-Salam, N. M., Khenata, R. (2017). Fabrication and characterization of 150 nm tin antimony sulfide thin films, a promising window layer material for homojunction solar cells. *Applied Physics A 123*, 282. https://doi.org/10.1007/s00339-017-0879-4

Ali, N., Hussain, A., Ahmed, R., Wang, M. K., Zhao, C., Haqa, B. U., Fu, Y. Q. (2016). Advances in nanostructured thin film materials for solar cell applications. *Renewable and Sustainable Energy Reviews 59*, 726-737. https://doi.org/10.1016/j.rser.2015.12.268

Aousgi, F. and Kanzari, M. (2011). Study of the optical properties of Sn-doped Sb_2S_3 thin films. *Energy Procedia 10*, 313-322.

Becerra, D., Nair, M. T. S. and Nair, P. K. (2011). Analysis of a bismuth sulfide/silicon junction for building thin film solar cells. *Journal of the Electrochemical Society 158*, H741-H749. https://doi.org/10.1149/1.3591045

Ben Rabeh, M., Khedmi, N., Kanzari, M. (2015). Prospect for $Sn_mSb_{2n}S_{3n+m}$ (n = 1, m = 1, 2, 3) sulfosalt compounds. *Journal of Materials Science: Materials in Electronics 26*, 2002-2009. https://doi.org/10.1007/s10854-014-2531-9

Bennaji, N., Fadhli, Y., Mellouki, I., Lahouli, R., Kanzari, M., Yacoubi, N., Khirouni, K. (2019). Thermal, electrical and dielectric characteristics of snsbs thin films for solar cell applications. *Journal of Electronic Materials 1*, 1-8. https://doi.org/10.1007/s11664-019-07782-7

Boldish, S. I., White, W. B. (1998). Optical band gaps of selected ternary sulfide minerals. *American Mineralogist 83*, 865-871. https://doi.org/10.2138/am-1998-7-818

Chalapathi, U., Poornaprakash, B., Ahn, C., Park, S. (2018). Large-grained Sb_2S_3 thin films with Sn-doping by chemical bath deposition for planar heterojunction solar cells. *Materials Science in Semiconductor Processing 84*, 138-143. https://doi.org/10.1016/j.mssp.2018.05.017

Cullity B. D., Stock, S. R. (2001). *Elements of X-ray Diffraction*. Pearson, London.

Dittrich, H., Bieniok, A., Brendel, U., Grodzicki, M., Topa, D. (2007). Sulfosalts-A new class of compound semiconductors for photovoltaic applications. *Thin solid films 515*, 5745-5750. https://doi.org/10.1016/j.tsf.2006.12.071

Dittrich, H., Stadler, A., Topa, D., Schimper, H. J., Basch, A. (2009). Progress in sulfosalt research. *Physica Status Solidi A: Applications and Materials Science 206*, 1034-1041. https://doi.org/10.1002/pssa.200881242

Drissi, N., Gassoumi, A., Boughzala, H., Ouerfellic, J., Kanzari, M. (2013). Investigation of structural and optical properties of the sulfosalt $SnSb_4S_7$ thin films. *Journal of Molecular Structure 1047*, 61-65. https://doi.org/10.1016/j.molstruc.2013.04.068

Fadhli, Y., Rabhi, A., Kanzari, M. (2016). Optical constant and electrical resistivity of annealed $Sn_3Sb_2S_6$ thin films. *Acta Metallurgica Sinica 29*, 287-294. https://doi.org/10.1007/s40195-016-0391-4

Garcia-Angelmo A. R., M.T.S. Nair and P. K. Nair (2014). Evolution of crystalline

structure in sns thin films prepared by chemical deposition. *Solid State Sciences 30*, 26-35. http://dx.doi.org/10.1016/j.solidstatesciences.2014.02.002

Gassoumi, A., Kanzari, M. (2011). Growth and post-annealing effect on the properties of the new sulfosalt $SnSb_2S_4$ thin films. P*hysica E: Low-dimensional Systems and Nanostructures 44*, 71-74. https://doi.org/10.1016/j.physe.2011.07.007

Gassoumi, A., Meradji, H., Kamoun-Turki, N., Ghemid, S. (2015). First principles study of electronic and optical properties of the ternary $SnSb_4S_7$ using modified Becke-Johnson potential. *Materials Science in Semiconductor Processing 40*, 262-266. https://doi.org/10.1016/j.mssp.2015.06.060

Hodes, G. (2003). *Chemically Solution Deposition of Semiconductor Films*. Marcel Dekker, Inc., New York.

Hodes, G. (2007). Semiconductor and ceramic nanoparticle films deposited by chemical bath deposition. *Physical Chemistry Chemical Physics 9*, 2181-2196. https://doi.org/10.1039/B616684A

Hubbell, J. H., Seltzer, S. M. (2004). NIST X-ray mass attenuation coefficient tables. http://physics.nist.gov/PhysRefData/XrayMassCoef/tab3.html, accessed 10 May 2016.

Jebali, A., Khemiri, N., Kanzari, M. (2016). The effect of annealing in N_2 atmosphere on the physical properties of $SnSb_4S_7$ thin films. *Journal of Alloys and Compounds 673*, 38-46.

Khan, M. A., Ahmed, A., Ali, N., Iqbal, T., Arif Khan, A., Ullah, M, Shafique, M. (2016). Improved optical properties of tin antimony sulphide thin films for photovoltaics. *American Journal of Materials Science and Engineering 4*, 1-6. http://pubs.sciepub.com/ajmse/4/1/1

Khemiri, N., Abdelkader, D., Jebali, A., Antoni, F., Kanzari, M. (2018). Effects of excimer laser annealing energy on the properties of thermally evaporated tin antimony sulfide thin films and TEM characterization of the powder. *Journal of Materials Science: Materials in Electronics 29*, 16295-16304. https://doi.org/10.1007/s10854-018-9719-3

Larbi, A., Akkari, F. C., Dahman, Demaille, H. D., Gallas, B. and Kanzari, M. (2016). Structural, morphological and optical properties of $Sn_3Sb_2S_6$ thin films synthesized by oblique angle deposition. *Journal of Electronic Materials 45*, 5487-5496. https://doi.org/10.1007/s11664-016-4714-z

Larbi, A., Dahman, H. and M. Kanzari (2014a). Effect of substrate temperature on structural and optical properties of the new high absorbent $Sn_3Sb_2S_6$ thin films. *Vacuum 110*, 34-39. http://dx.doi.org/10.1016/j.vacuum.2014.08.009

Larbi, A., Khedmi N. and M. Kanzari (2014b). The effect of the growth condition on the properties of the new material $Sn_3Sb_2S_6$ thin films. *International Journal of Thin Films Science and Technology 3*, 27-34.

Lee, W., Ki Min, S., Dhas, V., Ogale, S. B., Han, S. H. (2009). Chemical bath deposition of CdS quantum dots on vertically aligned ZnO nanorods for quantum dots-sensitized solar cells. *Electrochemistry Communications 11,* 103-106. https://doi.org/10.1016/j.elecom.2008.10.042

Lee, W., Lee, J., Lee, S., Yi, W., Han, S.H., Cho, B.W. (2008). Enhanced charge collection and reduced recombination of CdS/TiO_2 quantum-dots sensitized solar cells in the presence of single-walled carbon nanotubes. *Applied Physics Letters 92*, 153510. https://doi.org/10.1063/1.2911740

Madelung, O. (1992). *Data in Science and Technology, Semiconductors Other than Group IV Elements and III-V Compounds*. Springer-Verlag, Berlin.

McCandless, B. E. (2005). Glancing incidence X-ray diffraction of polycrystalline thin films. *Materials Research Society Symposium Proceedings 865*, 75-79. https://doi.org/10.1557/PROC-865-F4.1

Mellouki, I, Mami, A. Bennaji, N., Fadhli, Y. (2018). Study of doping and annealing effects on thermal properties of $Sn_xSb_2S_y$ ($1 \leq x \leq 3{,}4 \leq y \leq 6$) sulfosalts thin films by electro-pyroelectric

technique. *Thermochimica Acta 670*, 123-127. https://doi.org/10.1016/j.tca.2018.10.021

Musgraves, J. D., Carlie, N., Hu, J., Petit, L., Agarwal, A., Kimerling, L. C., Richardson, K. A. (2011). Comparison of the optical, thermal and structural properties of Ge-Sb-S thin films deposited using thermal evaporation and pulsed laser deposition techniques. *Acta Materialia 59,* 5032-5039. https://doi.org/10.1016/j.actamat.2011.04.060

Nair, P. K., Garcia-Angelmo, A. R., Nair, M. T. S. (2016). Cubic and orthorhombic SnS thin-film absorbers for tin sulfide solar cells. *Physica Status Solidi A 213*, 170-177. https://doi.org/10.1002/pssa.201532426

Nelson, J., (2003) *The Physics of Solar Cells*. Imperial College Press, London.

Ovando-Medina, V. M., Farías-Cepeda, L., Pérez-Aguilar, N. V., Rivera de la Rosa, H., Martínez-Gutiérrez, J., Romero Galarza, A., Cervantes-González, E., Cayetano-Castro, N. (2018). Facile synthesis of low band gap ZnO microstructures. *Revista Mexicana de Ingeniería Química 17*, 455-562. doi: 10.24275/10.24275/uam/izt/dcbi/revmexingquim/2018v17n2/Ovando

Rodríguez-Lazcano, Y., Nair, M. T. S., Nair, P. K. (2005). Photovoltaic p-i-n structure of Sb_2S_3 and $CuSbS_2$ absorber. *Journal of the Electrochemical Society 152*, G635-G638. https://dx.doi.org/10.1149/1.1945387

Schroder, D. K. (1990). *Semiconductor Materials and Device Characterization*. Wiley, New York.

Smith, R.A. (1978). *Semiconductors*. Cambridge University Press, Cambridge.

Tlig, F, Gannouni, M., Ben Assaker, I., Chtourou, R. (2017). New investigation on the physical and electrochemical properties of (TAS) thin films grown by electrodeposition technique. *Journal of Photochemistry and Photobiology A: Chemistry 13*, 26-35. https://doi.org/10.1016/j.jphotochem.2016.11.013

Würfel, P. (2005). *Physics of Solar Cells - From Principles to New Concepts*. Wiley-VCH, Weinheim.